Journal of Colloid and Interface Science 710 (2026) 140013

Contents lists available at ScienceDirect

Journal of Colloid And Interface Science

journal homepage: www.elsevier.com/locate/jcis

Halloysite nanotubes interacting with lipid vesicle membranes

Chiara Ferlito [a,*], Lorenzo Lisuzzo [a], Giuseppe Lazzara [a,*], Marc Schmutz [b], Antonio Stocco [b,*]

[a] Dipartimento di Fisica e Chimica Emilio Segrè, Università degli Studi di Palermo, Viale delle Scienze, pad. 17, 90128 Palermo, Italy
[b] Université de Strasbourg, CNRS UPR22 Institut Charles Sadron, 23 rue du Loess, Strasbourg, 67034, France

GRAPHICAL ABSTRACT

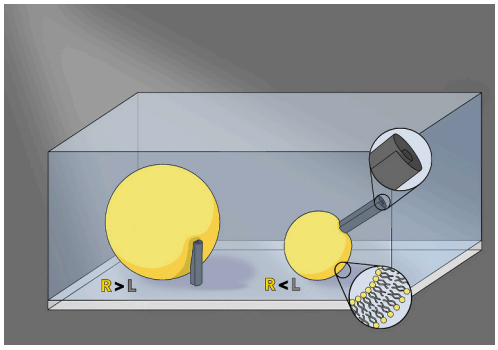

ARTICLE INFO

Keywords:
Halloysite nanotubes
Clays
Vesicles
Lipid membranes

ABSTRACT

Halloysite nanotubes (HNTs), naturally occurring aluminosilicates with a tubular structure, are promising nanocarriers for drug delivery due to their biocompatibility and unique morphology. However, their interaction with lipid membranes remains not fully explored. In this work, we aim at elucidating on the adhesion of HNTs on unilamellar vesicles made of phospholipids used as model of biological membranes. The adhesion was modulated by varying the lipid composition, ionic strength, and the size ratio between HNTs and vesicles. The adhesion mechanism was also studied by trapping a single HNT with optical tweezers and let it interact with a single vesicle. These findings show a preferential adhesion of the HNT tip on the lipid bilayer, which represents an important step toward directional membrane targeting in biomedical applications.

1. Introduction

Halloysite nanotubes (HNTs) are among the most widely studied and utilized nanoclays due to their unique hollow tubular structure and chemical similarity to kaolinite. This distinctive morphology, combined with its natural abundance, makes halloysite a versatile material for applications in several fields, including catalysis, environmental remediation, and nanomedicine [1–3]. Halloysite is a naturally occurring clay mineral from the kaolin group, first identified by Berthier as a 1:1 dioctahedral aluminosilicate [4]. What makes it different from its close relative kaolinite is the presence of interlayer water molecules, which play a key role in shaping its structure. Its general formula, $Al_2Si_2O_5(OH)_4{\cdot}nH_2O$, reflects this variability: when $n = 2$, it exists in the hydrated form known as halloysite 10 Å; when $n = 0$, it becomes the

* Corresponding authors.
E-mail addresses: chiara.ferlito01@unipa.it (C. Ferlito), giuseppe.lazzara@unipa.it (G. Lazzara), stocco@unistra.fr (A. Stocco).

https://doi.org/10.1016/j.jcis.2026.140013
Received 24 November 2025; Received in revised form 23 January 2026; Accepted 28 January 2026
Available online 29 January 2026

dehydrated form, halloysite 7 Å, typically achieved through heating or vacuum treatment [5,6]. Structurally, halloysite consists of alternating layers of silica tetrahedra and alumina octahedra, which roll up to form hollow nanotubes. The dimensions depend on the geological source and purification method, but they generally exhibit an internal diameter of 10–30 nm, an external diameter of 40–70 nm, and lengths of 200–4000 nm [7]. The internal structure of HNTs is highly complex, with edge steps present along both the tubular surface and the ends. These steps result in abrupt changes in the nanotube morphology and are associated with increased chemical reactivity, as atoms located at these edges are not fully coordinated [8]. This unique tubular morphology makes halloysite a highly versatile material with promising potential across a range of scientific and technological applications [9–11].

In recent years, HNTs have attracted growing interest as carriers for controlled drug delivery, thanks to their unique tubular structure, biocompatibility, and ability to encapsulate a wide variety of therapeutic agents [12]. Thanks to their tubular structure, HNTs can efficiently encapsulate drugs within their inner cavity, while their modifiable outer surface can be engineered to control release kinetics, improve targeted delivery, or activate release under specific pH. Cheng et al. reported an example of a halloysite hydrogel exhibiting hydrogen peroxide responsiveness and a turn-on fluorescence behavior, developed for controlled drug delivery [13,14].

Despite their promising biomedical applications, the behavior of HNTs in complex biological environments remains only partially understood. Their interactions with cellular membranes are crucial for evaluating both the efficacy and safety of drug delivery systems. When in contact with lipid bilayer membranes, micro and nanoparticles may induce poration or rupture, be internalized by the cell, or be repelled [15–17]. Some experiments were performed using giant unilamellar vesicles (GUVs), which offer highly suitable biomimetic platforms to investigate these interactions under controlled in vitro conditions. As synthetic cell-sized vesicles composed of lipid bilayers, GUVs allow direct observation of key processes such as nanoparticle adsorption, membrane penetration, deformation, or disruption [18,19].

Giant unilamellar vesicles are powerful model systems with applications spanning two main fields: membrane biophysics and the bottom-up construction of synthetic cells [20]. In the first context, they are employed to study phase separation, domain formation, membrane deformation, as well as interactions with proteins, peptides, and antimicrobial agents [21]. Within synthetic biology, GUVs have been engineered to mimic key cellular features such as compartmentalization, communication, growth, division, motility, and metabolic activity, enabling the development of artificial cells capable of interacting with living systems [22]. More recently, GUVs have also been explored as potential drug delivery vectors, particularly thanks to advances in microfluidic techniques that allow the efficient encapsulation of large biomolecules such as DNA, RNA, and enzymes [23,24].

A few studies still investigate the interaction between nanotubes and lipid vesicles. Notably, carbon nanotubes used in biomedical applications have demonstrated that variations in surface functionalization can lead to distinct modes of interaction with GUVs: they can localize on the membrane surface, interacting with the lipid headgroups, insert within the bilayer, interacting with the hydrophobic tails, or even induce the formation of micellar structures [25]. Carbon nanotubes with lengths of 5–15 nm have also been engineered to insert into lipid membranes, functioning as artificial channels for the transport of water, protons, small ions, and DNA [26]. Taking advantage of their tubular geometry, they can be treated as rigid rods, for which translational and rotational diffusion coefficients can be predicted based on their length and diameter using established theoretical frameworks [27]. Upon contact with a lipid membrane, their anisotropic shape and orientation give rise to two distinct engulfment pathways tip-first or side-first with membrane tension further modulating both the selection and progression of these pathways [28].

In this contest, we investigate the interactions between halloysite nanotubes (HNTs) and giant unilamellar vesicles (GUVs) using optical microscopy, particle tracking, and optical tweezers. Interactions can be enhanced either by tuning the surface properties of the nanotubes or by modifying the vesicles. For instance, alkaline treatments increase the number of external reactive OH groups on HNTs, strengthening hydrogen bonding and electrostatic interactions with lipid membranes, while surface functionalization with molecules such as silanes can introduce specific chemical groups to modulate these interactions. Alternatively, surface functionalization with molecules such as silanes can introduce specific chemical groups to modulate these interactions [29,30]. In this study, we focused on modifying the membrane composition or the ionic strength to enhance the attraction between nanotubes and membranes.

To gain further insight into these interactions at smaller length scales, we complement this approach with cryo-TEM analysis on analogous systems, employing small unilamellar vesicles (SUVs) and smaller HNTs. This system provides a well-defined model to study interactions, representing a preliminary step toward the potential use of halloysite nanotubes in biomedical applications.

2. Experimental study

2.1. Materials

Stock solutions of DOPC (1,2-dioleoyl-sn-glycero-3-phosphocholine), DOTAP (1,2-dioleoyl-3-trimethylammonium-propane), and NBD PE (1,2-dioleoyl-sn-glycero-3-phosphoethanolamine-N-(7-nitro-2-1,3-benzoxadiazol-4-yl)) were obtained from Avanti Polar Lipids. Two different vesicle systems were studied: neutral vesicles (99% DOPC, 1% NBD-PE) and cationic vesicles (95% DOPC, 4% DOTAP, 1% NBD-PE), prepared at molar ratios of 99:1 and 94:5:1, respectively, with a final lipid concentration of 1 g/L. Imerys Ceramics supplied halloysite nanotubes sourced from Matauri Bay, New Zealand (HNTs_NZ), whereas Hallo-Pure halloysite nanotubes (HNTs_UP) were obtained from I-Minerals. Both materials were utilized without further modification. Sodium chloride (NaCl, ≥99.0% purity), glucose (≥95.0%), and sucrose (≥99.5%) were purchased from Sigma-Aldrich.

3. Methods

The optical setup comprised a Nikon Eclipse TE2000 microscope (×60 objective; Nikon) equipped with a CMOS camera (OrcaFlash 4.0, Hamamatsu) working in bright field or fluorescence. Video acquisition was performed at frame rates ranging from 10 to 900 fps. The particle center of mass (x, y) was tracked using the open-source software ImageJ 1.54p. Tracking of HNT orientation was also performed by measuring the angle φ between the major axis of the tube and the horizontal axis in the imaging plane. The image analysis identified a brighter region corresponding to the HNT. The size of this bright region also depends on the out-of-plane particle orientation angle. For each experimental condition, including systems with NaCl and membranes containing DOTAP, 15–20 independent particle trajectories were analyzed. Trajectories were obtained from multiple vesicles and distinct areas of the sample, enabling the capture of the full range of interaction behaviors.

We used an optical tweezer setup that features a 976 nm fiber Bragg grating (FBG) single-mode laser diode (Thorlabs BL976-SAG300) with a maximum output power of 300 mW. This laser is coupled to a high numerical aperture objective lens (Nikon Plan Fluor 100×, NA = 1.30) to enable efficient optical trapping. Sample visualization is achieved through an LED illumination source paired with a CMOS camera (OrcaFlash 4.0, Hamamatsu). The system also includes a fluorescence module (Thorlabs OTKB-FL) integrated with a mercury lamp (Nikon C-HGFI) for fluorescence imaging.

The principle of Cryo-TEM of vitrified specimens was previously described by Dubochet et al. in 1988. The vitrification of the samples was carried out in a homemade vitrification system. The chamber was

maintained at 22 °C, and the relative humidity was 80%. A 5 μL drop of the sample was deposited onto a lacey carbon film covered with a 300 mesh Cu grid (Ted Pella-USA) rendered hydrophilic using an ELMO glow discharge unit (Cordouan Technologies, Pessac, France). The grid was automatically blotted to form a thin film and plunged in liquid ethane at −190 °C, as maintained by liquid nitrogen. Thus, a vitrified film was obtained in which the native structure of the nanoparticles and liposomes was preserved. The grid was mounted onto a cryo holder (Gatan 626-Pleasanton, CA, USA) and observed under low-dose conditions (10 e A [2]) in a Tecnai G2 microscope (FEI, Eindhoven, Netherlands) at 200 kV. Images were acquired using an Eagle slow scan CCD camera (FEI) [31].

3.1. Preparation of Giant unilamellar vesicles

Giant unilamellar vesicles (GUVs) were obtained using the polyvinyl alcohol (PVA) gel-assisted swelling method [32]. Briefly, a 5% (*w*/w) PVA solution was prepared in ultrapure water and stirred on a hot plate at 80 °C for 3 h. Subsequently, 100 μL of the solution was spread onto the bottom of a polytetrafluoroethylene (PTFE) chamber and dried in an oven at 80 °C for 35 min to form a thin gel film. Afterwards, 10 μL of lipid solution (as reported in 2.1. Materials) was spread onto the dried PVA film and placed under vacuum for 30 min to allow complete evaporation of chloroform.

The lipid-coated film obtained was hydrated with 200 μL of a 150 mM sucrose solution and incubated for 2 h, allowing vesicle formation through the swelling process [32]. The resulting GUVs suspension was subsequently transferred into an Eppendorf tube containing 1 mL of a 158 mM glucose solution. This created a slight osmolarity and density difference between the vesicle interior (sucrose solution) and exterior (glucose solution), promoting gentle deflation and sedimentation of the GUVs.

In addition, in some cases, the same preparation was carried out by adding NaCl to the sucrose and glucose solutions to reach a final concentration of 7 mM. This concentration was chosen as the minimum effective ionic strength capable of providing a measurable screening of electrostatic repulsion, thereby enabling a clearer enhancement and observation of the interactions between halloysite nanotubes and giant vesicles. In this case, the lipid mixture consisted of DOPC and NBD-PE in a 99:1 M ratio.

3.2. Preparation of small unilamellar vesicles

Small unilamellar vesicles (SUVs) were prepared using 100 μL of DOPC–DOTAP (10 mg/mL) placed in a 5 mL flask. Subsequently, 10 μL of a lipid solution in chloroform (1 mg/mL) was added, and the solvent was evaporated under reduced pressure (20 mbar) for 45 min. The resulting lipid film was hydrated with 1 μL of water and stored at 4 °C for 12 h. The sample was then subjected to five sonication cycles, followed by centrifugation at 4000 rpm for 10 min [33].

3.3. Sample for optical microscopy

A 0.17 mm-thick glass coverslip is first cleaned by sequential immersion in chloroform, acetone, ethanol, and ultrapure water baths, then dried with compressed air. For cationic vesicles, the glass is immersed for 15 min in a 2.5 g/L polyethylenimine (PEI) solution prepared in ultrapure water, followed by three rinses of 2 min each with ultrapure water. This treatment prevents positively charged vesicles from rupturing upon contact with the glass surface and is omitted when working with uncharged GUVs. A self-adhesive silicone isolator (9 mm diameter, 1.7 mm thickness) is then applied to the coverslip to form the sample chamber. The chamber is filled with 100 μL of 158 mM glucose solution, 10 μL of GUV suspension, and 1 μL of a 1 g/L particle suspension. Finally, the chamber is sealed with a second coverslip to maintain constant osmotic pressure, prevent water evaporation, and minimize convection effects. To study the interaction between single vesicles and nanotubes, a 0.001% HNTs suspension was added directly onto the vesicle sample after deposition with a micropipette.

3.4. Particle tracking and diffusion of cylindrical particles

To explore the interactions between single halloysite nanotubes and single giant vesicles, the nanotubes trajectories were first investigated in the absence of vesicles. For this purpose, images were first processed by adjusting contrast and brightness to clearly highlight the regions of the nanotubes without optical interference. In order to analyse the diffusion of HNTs, the particle is considered as a cylinder, with a long axis corresponding to the nanotube length L and a short axis corresponding to its diameter d.

In the bulk, diffusion coefficients of a cylindrical particle can be written as [27,34]:

$$D_{tr,\parallel}^{(b)} = \frac{k_B T[\ln(L|\mathrm{d}) + \gamma_{\parallel}]}{2\pi\eta L}$$

$$D_{tr,\perp}^{(b)} = \frac{k_B T[\ln(L|\mathrm{d}) + \gamma_{\perp}]}{4\pi\eta L}$$

$$D_{ro}^{(b)} = \frac{3k_B T[\ln(L|\mathrm{d}) + \gamma_{r}]}{\pi\eta L^3}$$

where k_B is the Boltzmann constant, T is the temperature and η is the fluid viscosity; $\gamma_{\parallel}$, $\gamma_{\perp}$ and γ_r are functions of the aspect ratio L/d.

Translational diffusion lengthwise $D_{tr,\parallel}^{(b)}$ is always higher than the sidewise diffusion $D_{tr,\perp}^{(b)}$, and for high aspect ratios, $D_{tr,\parallel}^{(b)}/D_{tr,\perp}^{(b)}$ tends to 2.

Experimental diffusion coefficients $D_{tr,\parallel}$ $D_{tr,\perp}$ and D_{ro} can be measured by the slopes of the mean squared displacements and angular displacements of the tube as a function of the lag time. Displacements can be measured in the lab frame (x, y) and in the rod frame (lengthwise a, and sidewise b) and angular displacement are calculated from the tube orientation angle φ:

$$\mathrm{MSD}_x + \mathrm{MSD}_y = <\Delta x^2 + \Delta y^2> = 2\left(D_{tr,\parallel} + D_{tr,\perp}\right)\Delta t$$

$$\mathrm{MSD}_a = <\Delta a^2> = 2D_{tr,\parallel}\Delta t$$

$$\mathrm{MSD}_b = <\Delta b^2> = 2D_{tr,\perp}\Delta t$$

$$\mathrm{MSAD} = <\Delta\varphi^2> = 2D_{ro}\Delta t$$

where Δt is the lag time.

4. Results and discussion

4.1. Halloysite nanotubes in aqueous solution.

Halloysite tubes show different size distributions depending on the source deposit. Two different halloysites were used in this study: HNTs-NZ and HNTs-UP (see section 2.1). A morphological characterization was carried out to assess the nanotube length distribution using dried samples in optical microscopy. As shown in **S1**, NZ allosite exhibits a shorter length, with over 60% of the particles ranging from 0.75 to 1.29 μm. In contrast, HNTs-UP are mostly composed of tubes with lengths showing significant distributions in the ranges 1.3–1.6 μm and 2–5 μm. Regarding the tube diameter, typical distributions in the range between 60 and 160 nm were measured by electron microscopy for both tube types. Optical microscopy cannot resolve structures at this diameter scale, and the measurements obtained are approximately six times larger than those from electron microscopy due to the light-scattering halo of the tubes. Considering the size differences among the HNTs, we have investigated HNTs-UP interacting with giant lipid vesicles by optical

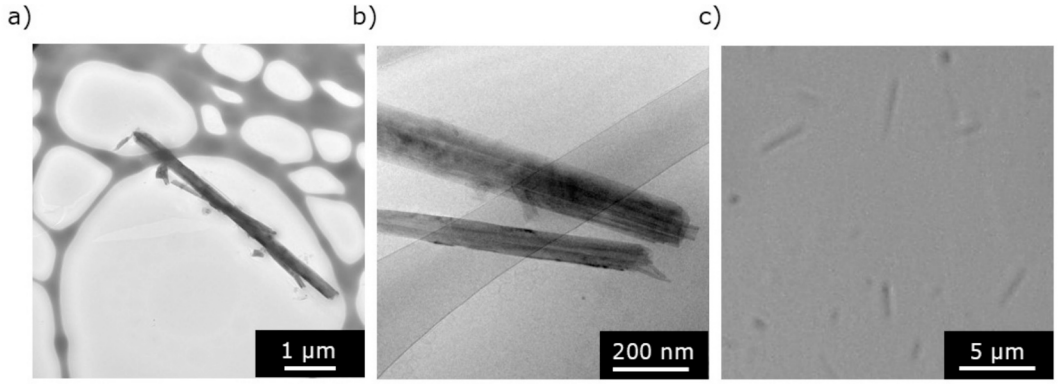

Fig. 1. (a) TEM images of HNTs-UP (b) TEM images of HNTs-NZ (c) Optical microscopy image of HNTs-UP.

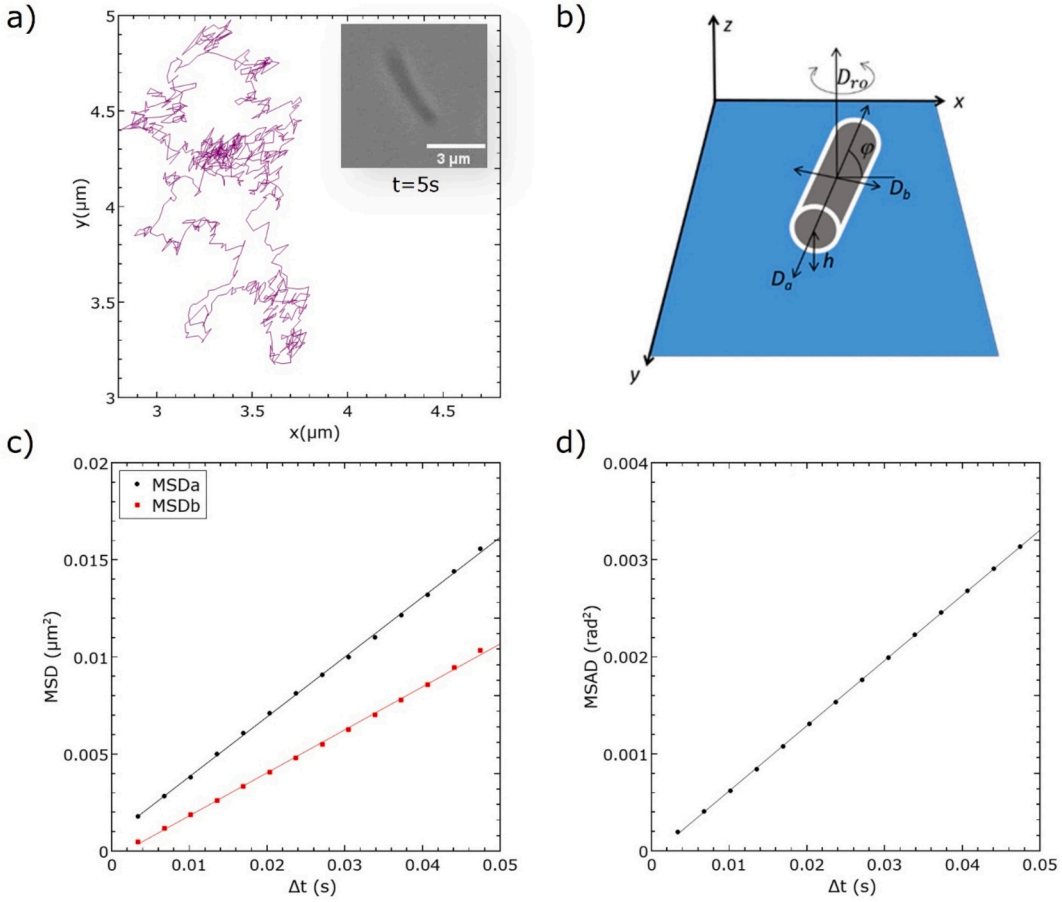

Fig. 2. a) Center of mass trajectory of a HNT-UP in the *xy* lab. Inset shows an optical microscopy image of a tube laying parallel to the bottom wall; b) Schematic representation of the nanotube motion along its length (*a*) and side (*b*); c) MSD along the major axis (MSD_a) and minor axis (MSD_b); d) MSAD as a function of the lag time. Lines are linear fits to measure the diffusion coefficients.

microscopy and HNTs-NZ interacting with small unilamellar vesicles by electron microscopy. (Fig. 1).

4.2. Brownian motion of long Halloysite nanotubes in aqueous solutions

The dynamics of several single HNTs-UP in water were analyzed to establish a baseline before examining their interactions with GUVs. We have focused our attention on tubes with $L \geq 4$ μm. An example of the measured trajectories is shown in Fig. 2. Given the length and the density of HNTs-UP, tubes lay parallel to the bottom wall and perform Brownian motion, as shown in Fig. 2**-a** (S.4, video 1**)**. Mean squared displacements MSD_a and MSD_b are shown in Fig. 2**-c** reveal a clear anisotropy in its translational motion with a faster diffusion lengthwise $D_{tr,\parallel}$ than sidewise $D_{tr,\perp}$. This behavior is consistent with the hydrodynamic predictions.The mean squared angular displacement shown in Fig. 2**-d** is also linear with the lag time, and allows to measure the rotational diffusion coefficient D_{ro}, see SI.

Averaging on measurements with comparable tube lengths, we obtained $D_{tr,\parallel} = 0.22 \pm 0.06$ μm^2/s and $D_{tr,\perp} = 0.13 \pm 0.07$ μm^2/s, and $D_{ro,\parallel} = 0.07 \pm 0.06$ rad^2/s (see SI).

It should be noted that the measurement of the tube displacement sidewise could present a lower degree of accuracy, given the difference

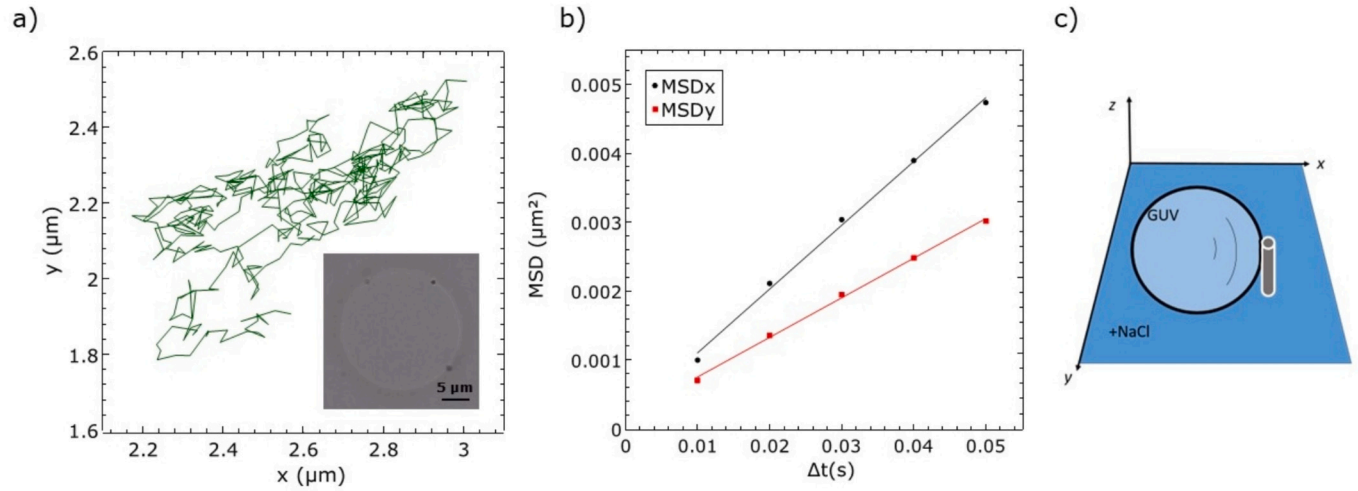

Fig. 3. Interaction between HNT and GUV in NaCl solution 7 mM (a) Nanotube trajectory in the *xy* plane along the GUV surface; (top right) optical microscopy image; (bottom right) sketch of the top view geometry; (b) Mean square displacement (MSD) of the nanotube in the x and y directions (c) preferential orientation of HNT.

between the diameter size $d \leq 160$ nm (by electron microscopy) and the apparent diameter d_{app} seen by optical microscopy $d_{app} \approx 6d$. Comparing the measured diffusions to the predicted bulk values for a typical aspect ratio $p = L/d = 30$ [27,34], we observe a slowing down of the diffusions, agreeing with the expected enhanced drag due to the vicinity to a solid wall. We find the ratios $D_{tr,\parallel}/D^{(b)}_{tr,\parallel} = 0.46 \pm 0.13$, $D_{tr,\perp}/D^{(b)}_{tr,\perp} = 0.41 \pm 0.22$ and $D_{ro}/D^{(b)}_{ro} = 0.54 \pm 0.22$. From these ratios, it is possible to evaluate the height of the tube axis with respect to the bottom wall [35]:

$$h = \frac{d}{2}\cosh\frac{D_i}{D_i^{(b)}},$$

which leads to $h \approx 0.56\, d$. Assuming $d = 160$ nm, the height of the HNT axis with respect to the bottom wall can be calculated: $h \approx 90$ nm, and the gap between the bottom of the tube and the wall would correspond to $h - d/2 \approx 10$ nm.

For HNTs-UP showing $L < 4$ µm, we observe very similar dynamics as in Fig. 2. However, being the tube gravity now comparable to the thermal agitation energy, we could observe that the tubes not only diffuse lengthwise parallel to the bottom wall, but they can also temporarily stand up, showing rotational dynamics out of the imaging plane.

4.3. Adhesion of HNTs on vesicle membranes by tuning the ionic strength of the aqueous solution

A preliminary study was conducted on HNTs-UP and GUVs composed of non-charged lipids such as DOPC. In this case, no significant change in the tube Brownian motion was observed with respect to the dynamics described before in the absence of vesicles. Hence, no spontaneous adhesion between HNTs-UP and DOPC lipid membranes was observed. Two strategies were applied to support adhesion between HNTs and GUVs. The first one involved adding NaCl to the inner and outer solutions of DOPC GUVs. By increasing the ionic strength of the solution, a screening of the electrostatic double layer repulsion between the tube and the membrane is expected. This reduction in the repulsion allows the nanotubes to come closer to the GUV membrane, and eventually, it could support the adhesion between the HNT and the lipid

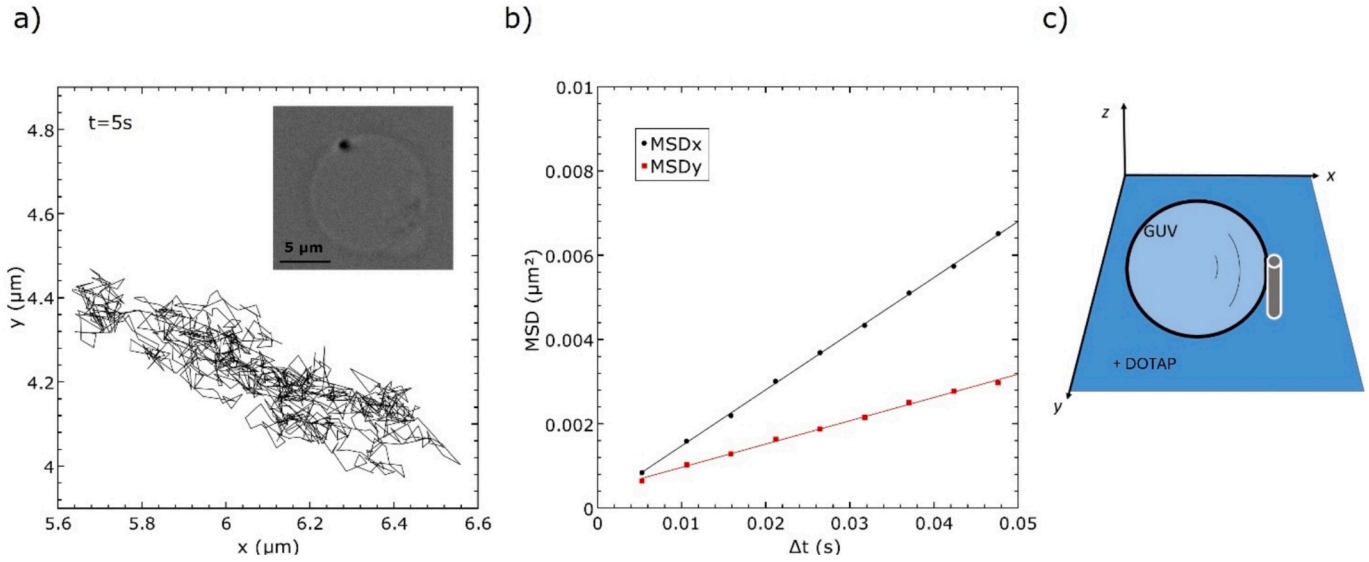

Fig. 4. a) (left) Tracking of a HNT interacting with cationic GUV (DOPC/DOTAP) by (top right) optical microscopy. (bottom right) sketch of the top view geometry; b) Mean square displacement (MSD) along the x-axis and the y-axis.

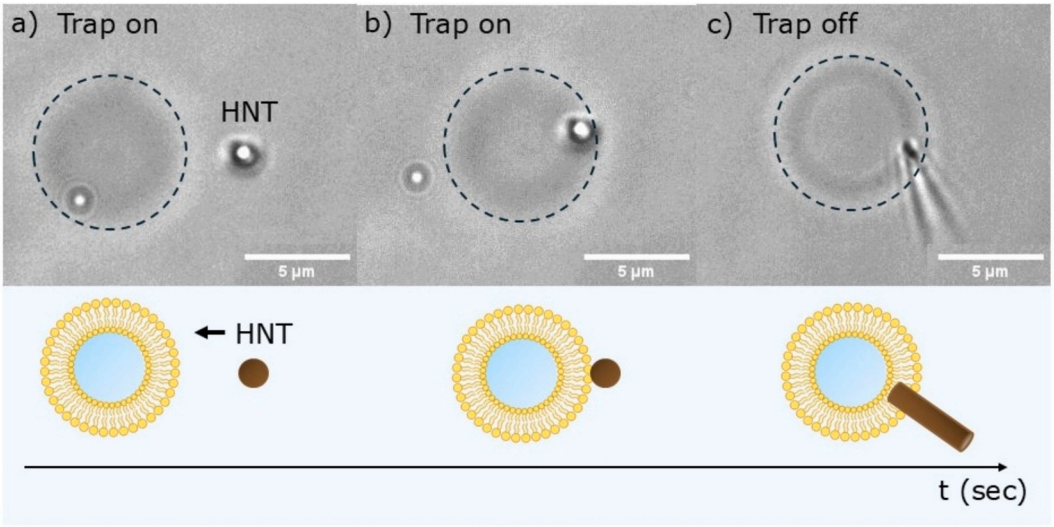

Fig. 5. Selected frames from optical tweezers recording, showing the initial contact between cationic GUV and HNT tip.

bilayer.

We start investigating large GUVs showing radii larger than 5 µm (> *L*) in 7 mM NaCl aqueous solutions. In optical microscopy, a surprising result was to observe that not only a HNT-UP adheres to a GUV in the presence of salt, but that the adhesive HNT appears as circular objects rather than long cylinders, **see** Fig. 3. Hence, HNT stands up when they adhere to the GUV membrane. By analysing the tube trajectory, we observed that the HNT keeps its circular shape, and for large GUV, we did not observe any tube out-of-plane rotational dynamics, see (S4, Video 2). Hence, we could track the center of the tube axis in time (Fig. 3a), which follows an arc of the GUV surface.

From the measured mean squared displacements in the lab frame (x, y), see Fig. 3b, we calculate the translational diffusion of the tube on the GUV membrane $(D_{tr,x} + D_{tr,y})/2$, $D_{tr,x} = 0.05$ µm^2/s and $D_{tr,x} = 0.03$ µm^2/s. From these values, it follows that the tube diffusion on the membrane is significantly smaller than both the bulk prediction $D^{(b)}_{tr,\perp}$ (see SI) and the measured $D_{tr,\perp} = 0.13 \pm 0.07$ µm^2/s for a tube close to a solid wall.

This finding provides clear evidence of the confined dynamics of the nanotube at the vesicle interface where the local viscosity probed by the tube includes the membrane viscosity (local 3D viscosity ≈ 1 Pa.s) [18] rather than only the water viscosity (10^{-3} Pa.s) as in the free Brownian motion of a tube in water. No membrane fully wrapping the tube and no tube penetration inside the GUV were observed. The HNT-GUV interaction does not alter the shape and size of the vesicle, indicating the absence of strong deformation, damage, or disruption of the phospholipid bilayer. These observations will be discussed in terms of a preferential adhesion of the HNT tip, where the silanolic groups on the HNT surface engage with the polar headgroups of the lipids.

4.4. Adhesion of HNTs on vesicle membranes by tuning the membrane composition

The second strategy to support adhesion between HNTs and GUV is by the incorporation of DOTAP (4%) into the membrane composition, see Fig. 4 and S4. video 3.

From the trajectory shown in Fig. 4, as before we observe that the HNT stands up. By tracking the tube axis, we determine the diffusion coefficients of the tube on the GUV surface: $D_{tr,x} = 0.06$ µm^2/s and $D_{tr,y} = 0.02$ µm^2/s. Hence $(D_{tr,x} + D_{tr,y})/2$ is comparable with the values found for DOPC GUV in the presence of 7 mM NaCl. In this configuration, the adhesion between HNTs and GUVs can be attributed to the presence of DOTAP, a cationic lipid that confers an overall positive surface charge to the GUVs. Consequently, the vesicles exhibit a positive zeta potential of approximately +33 mV, which promotes electrostatic attraction with the negatively charged HNTs [18]. Despite differences in chemical composition, their zeta potentials are comparable (−24.5 and − 26.5 mV). In both cases, the nanotubes adopt the same preferential orientation, remaining upright and interacting with the membrane, consistent with the behavior observed previously.

4.5. Preferential tube tip–membrane adhesion of different HNTs on lipid vesicles

To verify our hypothesis of a preferential HNT tip adhesion on the lipid membrane and discuss a possible mechanism explaining the vertical position adopted by the HNT, we performed optical tweezers and electron microscopy experiments using vesicles of radii comparable or smaller than the tube length.

In the first experiments, we trapped a single HNT-UP nanotube by optical tweezers and investigated the adhesion kinetics on a cationic GUV. This approach provides direct visualization of the HNT–GUV interactions through the tip adhesion of an individual nanotube.

In these experiments, we used GUVs whose diameters are comparable to the tube length, $d_{GUV} \approx L$. As shown in Fig. 5, a nanotube is trapped in a stand-up position by optical tweezers. When the HNT is brought close to a GUV, no interaction is initially observed. Within few seconds, however, the nanotube adheres irreversibly to the membrane. After switching off the trap, the nanotube remains attached to the GUV. Once the adhesion occurs, it is not possible to remove the HNT from the GUV by applying optical forces in the pN range. In contrast to previous observations, when the vesicle size is significantly smaller than the nanotube length, the nanotube tip establishes direct interaction with the lipid membrane. Upon deactivation of the optical trap, the elongated side of the cylindrical structure becomes visible, highlighting that the vesicle radius is comparable to the nanotube length. Under these conditions, out-of-plane rotational dynamics can be clearly observed, and the nanotube no longer appears as a circular object (S4.Video 4). This result confirms the presence of a spontaneous and stable interaction between the nanotubes and the lipid membrane in the presence of DOTAP. The observed behavior can be explained by the higher density of hydroxyl groups at the tips of HNTs, which enhances their interaction with the polar headgroups of lipid membranes. Such enrichment originates from the natural termination of the nanotube structure, where the crystallographic arrangement exposes more reactive hydroxyl groups at the ends than on the side walls. This chemical feature accounts for the preferential adhesion observed at the nanotube tips [36].

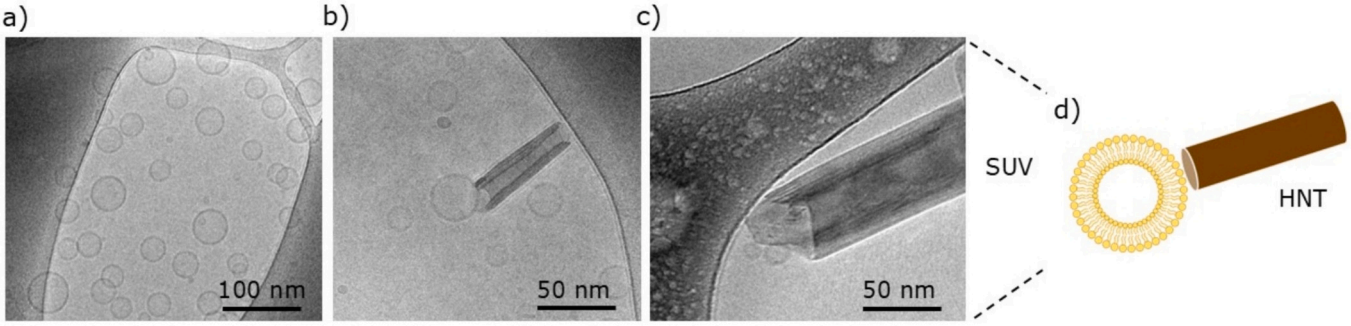

Fig. 6. (a) Cryo-TEM image of SUVs (4% DOTAP). (b-c) Cryo-TEM images showing the interaction between HNTs and SUVs, with a schematic illustration (d) of the interaction occurring at the nanotube edge.

To further investigate the interaction of HNTs at a smaller scale, small unilamellar vesicles (SUVs), were prepared and incubated with HNTs-NZ at a concentration of 7 mM of NaCl (Fig. 6**a).** In this case, we focus on vesicles that are smaller than the HNT length, $d_{SUV} < L$. Similarly to GUVs ($d_{GUV} > L$), no interaction was detected with neutral vesicles composed exclusively of DOPC. In contrast, incorporating DOTAP into the lipid composition led to an irreversible interaction, as confirmed by cryo-TEM images clearly showing the nanotube edges in contact with the vesicle bilayer. (Fig. 6 **b-c**). The presence of a lipid bilayer on the sides of the tubes can be observed, similarly to what has been reported for silica nanoparticles. This occurs through the spreading of lipid patches, which expand and coalesce to form a continuous bilayer, even over the irregular surface of the nanotubes [37]. This finding demonstrates that the interaction between HNTs and phospholipid membranes occurs preferentially on the tip of HNTs (HNTs-NZ and HNTs-UP), both for giant and small vesicles.

Finally, we wish to comment on the mechanism dictating the stand-up HNT position observed when long tubes interact with large vesicles ($d_{GUV} > L$), see Fig. 3 and fig. 4. Our observations point to a tube tip adhesion that moves against the gravity following the vertical profile of the vesicle. The lack of the out-of-plane rotational dynamics of the tube may indicate a possible weak pinning effect and a preferential interaction of the HNT tip on the bottom glass wall, which is only ≈ 10 nm (see section 3.2) from the HNT tip. This stand-up position observed in the absence of membrane wrapping is very different from the ones recently reported for large particles partially or fully wrapped by GUVs [28]. The different tip shape and the lack of membrane partial or full wrapping can be invoked to explain our results.

5. Conclusions

In this article, we investigated the interactions between halloysite nanotubes and lipid membranes using giant unilamellar vesicles and small unilamellar vesicles as biomimetic cell systems. The adhesion between HNTs and lipid vesicles can be controlled by screening the electric double layer repulsion by adding NaCl and by modulating the membrane potential through the addition of a cationic lipid in the composition. When the vesicle size is much larger than the HNT length, the nanotubes preferentially orient in a standing upright position rather than lying flat on the solid substrate. In this configuration, the interaction between the HNT and the membrane occurs on the nanotube tip. Optical tweezers experiment further reveal the irreversible nature of the HNT–GUV adhesion, characterized by a tip adhesion mechanism. Finally, for vesicles smaller than the HNTs, cryo-TEM images confirm the nanotube tip adhesion on the lipid bilayers. These findings demonstrate that HNT–membrane tip adhesion occurs in very different geometries and can be controlled by electrostatic interactions. Beyond providing fundamental insights into the behavior of HNTs in biological environments, this study contributes to the broader understanding of nanotube membrane dynamics, which is essential for the safe and effective development of nanomaterials in biomedical and environmental applications.

Supplementary data to this article can be found online at https://doi.org/10.1016/j.jcis.2026.140013.

CRediT authorship contribution statement

Chiara Ferlito: Writing – review & editing, Writing – original draft, Methodology, Investigation, Formal analysis, Data curation, Conceptualization. **Lorenzo Lisuzzo:** Writing – review & editing, Supervision, Conceptualization. **Giuseppe Lazzara:** Writing – review & editing, Validation, Supervision, Conceptualization. **Marc Schmutz:** Writing – review & editing, Validation, Supervision, Conceptualization. **Antonio Stocco:** Writing – review & editing, Supervision, Methodology, Funding acquisition, Data curation, Conceptualization.

Declaration of competing interest

The authors declare that they have no known competing financial interests or personal relationships that could have appeared to influence the work reported in this paper.

Acknowledgements

The authors would like to express their gratitude to Azeline Hilaire, Thomas Dartige, and the Mcube team at ICS, University of Strasbourg. CF thanks PR FSE + Sicilia 2021–2027. The ICS microscopy platform PLAMICS is also acknowledged.

Data availability

Data will be made available on request.

References

[1] C. Ferlito, C. Rizzo, R. Merir, G. Cavallaro, L. Lisuzzo, A.P. Piccionello, G. Lazzara, Influence of Halloysite nanotubes from different deposits on the degradation of organic molecules, Ceram. Int. (2025), https://doi.org/10.1016/j.ceramint.2025.02.403. S0272884225010995.
[2] H. Chen, W. Song, B. Zhang, Z. Zhang, Y. Yang, L. Bai, Y. Wu, H. Zhang, Halloysite-based X-ray-activated persistent luminescent hydrogels enable multiple-level encryption and dual-locked camouflage, Energy & Environ. Mater. 8 (5) (2025) e70034, https://doi.org/10.1002/eem2.70034.
[3] L. Zeng, X. Chen, S. Zhou, D. Zhang, B. Luo, C. Zhou, M. Liu, FeS2 Nanozymes@halloysite clay nanotube/polyvinyl alcohol/sodium alginate composite hydrogel for hemostasis and bacterial-infected wound healing, J. Colloid Interface Sci. 703 (2026) 139120, https://doi.org/10.1016/j.jcis.2025.139120.
[4] Berthirt P. Berthier, P. Analyse de l'halloysite, Ann. Chim. Phys. 32 (1826) 332–335.
[5] G. Cavallaro, L. Chiappisi, P. Pasbakhsh, M. Gradzielski, G. Lazzara, A structural comparison of Halloysite nanotubes of different origin by small-angle neutron scattering (SANS) and electric birefringence, Appl. Clay Sci. 160 (2018) 71–80, https://doi.org/10.1016/j.clay.2017.12.044.

[6] L. Lisuzzo, G. Cavallaro, S. Milioto, G. Lazzara, Halloysite nanotubes as Nanoreactors for heterogeneous micellar catalysis, J. Colloid Interface Sci. 608 (2022) 424–434, https://doi.org/10.1016/j.jcis.2021.09.146.
[7] M.M. Calvino, G. Cavallaro, L. Lisuzzo, S. Milioto, G. Lazzara, Separation of Halloysite/kaolinite mixtures in water controlled by sucrose addition: the influence of the attractive forces on the sedimentation behavior, Colloids Surf. A Physicochem. Eng. Asp. 641 (2022) 128530, https://doi.org/10.1016/j.colsurfa.2022.128530.
[8] N. Gray-Wannell, P. Cubillas, Z. Aslam, P.J. Holliman, H.C. Greenwell, R. Brydson, E. Delbos, L.-J. Strachan, M. Fuller, S. Hillier, Morphological features of Halloysite nanotubes as revealed by various microscopies, Clay Miner. 58 (4) (2023) 395–407, https://doi.org/10.1180/clm.2023.37.
[9] E. Abdullayev, Y. Lvov, Halloysite clay nanotubes as a ceramic "skeleton" for functional biopolymer composites with sustained drug release, J. Mater. Chem. B 1 (23) (2013) 2894, https://doi.org/10.1039/c3tb20059k.
[10] N.R. Abubakirov, R.F. Fakhrullin, Mathematical model of random walk of Halloysite nanotubes, Lobachevskii J Math 44 (11) (2023) 4587–4591, https://doi.org/10.1134/S1995080223110033.
[11] H. Zhang, B. Zhang, C. Cai, K. Zhang, Y. Wang, Y. Wang, Y. Yang, Y. Wu, X. Ba, R. Hoogenboom, Water-dispersible X-ray scintillators enabling coating and blending with polymer materials for multiple applications, Nat. Commun. 15 (1) (2024) 2055, https://doi.org/10.1038/s41467-024-46287-8.
[12] M. Fizir, P. Dramou, N.S. Dahiru, W. Ruya, T. Huang, H. He, Halloysite nanotubes in analytical sciences and in drug delivery: a review, Microchim. Acta 185 (8) (2018) 389, https://doi.org/10.1007/s00604-018-2908-1.
[13] X. Lei, Y. Zhou, X. Liu, L. Kong, L. Liao, Y. Li, M. Liu, L. Tian, W. Rao, G. Lv, Effective pH-responsive Nanocarrier based on the anisotropic surfaces of Halloysite nanotubes for controlled drug release, Applied Clay Science 232 (2023) 106799, https://doi.org/10.1016/j.clay.2022.106799.
[14] C. Cheng, Y. Gao, W. Song, Q. Zhao, H. Zhang, H. Zhang, Halloysite nanotube-based H2O2-responsive drug delivery system with a turn on effect on fluorescence for real-time monitoring, Chem. Eng. J. 380 (2020) 122474, https://doi.org/10.1016/j.cej.2019.122474.
[15] S. Zhang, H. Gao, G. Bao, Physical principles of nanoparticle cellular endocytosis, ACS Nano 9 (9) (2015) 8655–8671, https://doi.org/10.1021/acsnano.5b03184.
[16] J. Agudo-Canalejo, R. Lipowsky, Critical particle sizes for the engulfment of nanoparticles by membranes and vesicles with bilayer asymmetry, ACS Nano 9 (4) (2015) 3704–3720, https://doi.org/10.1021/acsnano.5b01285.
[17] M. Walczak, R.A. Brady, L. Mancini, C. Contini, R. Rubio-Sánchez, W.T. Kaufhold, P. Cicuta, L. Di Michele, Responsive Core-Shell DNA particles trigger lipid-membrane disruption and Bacteria entrapment, Nat. Commun. 12 (1) (2021) 4743, https://doi.org/10.1038/s41467-021-24989-7.
[18] C. Marque, G. D'Avino, D. Larobina, A. Michel, A. Abou-Hassan, A. Stocco, Diffusion of a single colloid on the surface of a Giant vesicle and a droplet, Phys. Rev. E 111 (2) (2025) 025411, https://doi.org/10.1103/PhysRevE.111.025411.
[19] V. Sharma, C.M. Marques, A. Stocco, Driven engulfment of Janus particles by Giant vesicles in and out of thermal equilibrium, Nanomaterials 12 (9) (2022) 1434, https://doi.org/10.3390/nano12091434.
[20] K.S. Nair, H. Bajaj, Advances in Giant Unilamellar vesicle preparation techniques and applications, Adv. Colloid Interface Sci. 318 (2023) 102935, https://doi.org/10.1016/j.cis.2023.102935.
[21] S.L. Veatch, S.L. Keller, Separation of liquid phases in Giant vesicles of ternary mixtures of phospholipids and cholesterol, Biophys. J. 85 (5) (2003) 3074–3083, https://doi.org/10.1016/S0006-3495(03)74726-2.
[22] C. Love, J. Steinkühler, D.T. Gonzales, N. Yandrapalli, T. Robinson, R. Dimova, T.-Y.D. Tang, Reversible pH-responsive Coacervate formation in lipid vesicles activates dormant enzymatic reactions, Angew. Chem. Int. Ed. 59 (15) (2020) 5950–5957, https://doi.org/10.1002/anie.201914893.
[23] A. Al-Atta, F. Sher, A. Hazafa, A. Zafar, H.M.N. Iqbal, E. Karahmet, E. Lester, Supercritical water oxidation of phenol and process enhancement with in situ formed Fe2O3 Nano catalyst, Environ. Sci. Pollut. Res. 29 (41) (2022) 61896–61904, https://doi.org/10.1007/s11356-021-16390-0.
[24] V. Noireaux, A. Libchaber, A vesicle bioreactor as a step toward an artificial cell assembly, Proc. Natl. Acad. Sci. U. S. A. 101 (51) (2004) 17669–17674, https://doi.org/10.1073/pnas.0408236101.
[25] V. Pérez-Luna, C. Moreno-Aguilar, J.L. Arauz-Lara, S. Aranda-Espinoza, M. Quintana, Interactions of functionalized Multi-Wall carbon nanotubes with Giant phospholipid vesicles as model cellular membrane system, Sci. Rep. 8 (1) (2018) 17998, https://doi.org/10.1038/s41598-018-36531-9.
[26] J. Geng, K. Kim, J. Zhang, A. Escalada, R. Tunuguntla, L.R. Comolli, F.I. Allen, A. V. Shnyrova, K.R. Cho, D. Munoz, Y.M. Wang, C.P. Grigoropoulos, C.M. Ajo-Franklin, V.A. Frolov, A. Noy, Stochastic transport through carbon nanotubes in lipid bilayers and live cell membranes, Nature 514 (7524) (2014) 612–615, https://doi.org/10.1038/nature13817.
[27] M.M. Tirado, C.L. Martínez, J.G. De La Torre, Comparison of theories for the translational and rotational diffusion coefficients of rod-like macromolecules. Application to short DNA fragments, J. Chem. Phys. 81 (4) (1984) 2047–2052, https://doi.org/10.1063/1.447827.
[28] S. Van Der Ham, J. Agudo-Canalejo, H.R. Vutukuri, Role of shape in particle-lipid membrane interactions: from surfing to full engulfment, ACS Nano 18 (15) (2024) 10407–10416, https://doi.org/10.1021/acsnano.3c11106.
[29] F. Ferrante, M. Bertini, C. Ferlito, L. Lisuzzo, G. Lazzara, D. Duca, A computational and experimental investigation of Halloysite silicic surface modifications after alkaline treatment, Applied Clay Science 232 (2023) 106813, https://doi.org/10.1016/j.clay.2022.106813.
[30] L. Lisuzzo, M. Bertini, G. Lazzara, C. Ferlito, F. Ferrante, D. Duca, A computational and experimental investigation of the anchoring of Organosilanes on the Halloysite silicic surface, Appl. Clay Sci. 245 (2023) 107121, https://doi.org/10.1016/j.clay.2023.107121.
[31] J. Dubochet, M. Adrian, J.-J. Chang, J.-C. Homo, J. Lepault, A.W. McDowall, P. Schultz, Cryo-Electron microscopy of vitrified specimens, Q. Rev. Biophys. 21 (2) (1988) 129–228, https://doi.org/10.1017/S0033583500004297.
[32] A. Weinberger, F.-C. Tsai, G.H. Koenderink, T.F. Schmidt, R. Itri, W. Meier, T. Schmatko, A. Schröder, C. Marques, Gel-assisted formation of Giant Unilamellar vesicles, Biophys. J. 105 (1) (2013) 154–164, https://doi.org/10.1016/j.bpj.2013.05.024.
[33] K. Mebrouk, M. Ciancone, T. Vives, S. Cammas-Marion, T. Benvegnu, C. Le Goff-Gaillard, Y. Arlot-Bonnemains, M. Fourmigué, F. Camerel, Fine and clean Photothermally controlled NIR drug delivery from biocompatible nickel-bis (Dithiolene)-containing liposomes, ChemMedChem 12 (21) (2017) 1753–1758, https://doi.org/10.1002/cmdc.201700344.
[34] G. Li, J.X. Tang, Diffusion of actin filaments within a thin layer between two walls, Phys. Rev. E 69 (6) (2004) 061921, https://doi.org/10.1103/PhysRevE.69.061921.
[35] A.J. Hunt, F. Gittes, J. Howard, The force exerted by a single kinesin molecule against a viscous load, Biophys. J. 67 (2) (1994) 766–781, https://doi.org/10.1016/S0006-3495(94)80537-5.
[36] L. Lisuzzo, L. Guercio, G. Cavallaro, D. Duca, F. Ferrante, Halloysite clay nanotubes for catalytic conversion of biomass: synergy between computational modeling and experimental studies, ACS Catal. 14 (23) (2024) 18167–18203, https://doi.org/10.1021/acscatal.4c05907.
[37] S. Mornet, O. Lambert, E. Duguet, A. Brisson, The formation of supported lipid bilayers on silica nanoparticles revealed by Cryoelectron microscopy, Nano Lett. 5 (2) (2005) 281–285, https://doi.org/10.1021/nl048153y.